

DR EHSAN TAHERI-NASSAJ (Orcid ID : 0000-0002-5342-9113)

PROFESSOR NATHAN NEWMAN (Orcid ID : 0000-0003-2819-9616)

Article type : Article

Corresponding author mail id :Nathan.Newman@asu.edu

### Origin of dielectric loss in $\text{Ba}(\text{Co}_{1/3}\text{Nb}_{2/3})\text{O}_3$ microwave ceramics

Ahmad Sayyadi-Shahraki<sup>1</sup>, Ehsan Taheri-Nassaj<sup>1</sup>, Hassan Sharifi<sup>2</sup>, Justin Gonzales<sup>4</sup>, Taras Kolodiazny<sup>3</sup>, and Nathan Newman<sup>4,\*</sup>

<sup>1</sup> Department of Materials Science and Engineering, Tarbiat Modares University, Tehran, PO Box 14115-143, Iran

<sup>2</sup> Department of Materials Science, Faculty of Engineering, University of Shahrekord, Shahrekord, 8815648456, Iran

<sup>3</sup> National Institute for Materials Science, 1-1 Namiki, Tsukuba, Ibaraki 305-0044, Japan

<sup>4</sup> Materials Program, Arizona State University, Tempe, Arizona 85287-6106, USA

#### Abstract

The microwave dielectric loss of stoichiometric and non-stoichiometric  $\text{Ba}(\text{Co}_{1/3}\text{Nb}_{2/3})\text{O}_3$  ceramics have been measured from 2-300 K in magnetic fields ranging from 0 to 5 T using a dielectric resonator (DR) technique. The microwave absorption from spin excitations of

---

\* Corresponding author. Tel.: +14807276934; Fax: +14807279321. Email address: Nathan.Newman@asu.edu (Nathan Newman).

This article has been accepted for publication and undergone full peer review but has not been through the copyediting, typesetting, pagination and proofreading process, which may lead to differences between this version and the Version of Record. Please cite this article as doi: 10.1111/jace.15343

This article is protected by copyright. All rights reserved.

unpaired d-electrons in exchange coupled  $\text{Co}^{2+}$  ions dominate the loss of the  $\text{Ba}(\text{Co}_{1/3}\text{Nb}_{2/3})\text{O}_3$  ceramics at cryogenic temperatures. Two peaks in the loss tangent ( $\tan \delta$ ) versus temperature relation from a distinctly different origin occur at 25-30 K and 90 K, which increase in magnitude with increasing Co content in the bulk dielectric samples. Evidence that these peaks result from polaron conduction from hopping between  $\text{Co}^{2+}$  and  $\text{Co}^{3+}$  ions includes (1) the peak's observed temperature range, (2) the decrease in peak intensity of approximately a factor of two in a large applied magnetic fields (5 T), and (3) a strong correlation between the peak's magnitude and both the fraction of the minority  $\text{Co}^{3+}$  in the dominant  $\text{Co}^{2+}$  matrix and D.C. conductivity at elevated temperatures. A magnetic-field independent high temperature peak with a maximum at 250 K dominates the room temperature microwave loss whose magnitude correlates with those of the low temperature peaks. This suggests that the defects responsible for carrier conduction play an important role in establishing the loss tangent at room temperature.

**Keywords:** Complex perovskite; Dielectric loss; Point defect; Dipole relaxation; Microwave resonator

## I. Introduction

Dielectric ceramics with complex perovskite crystal structure and  $\text{Ba}(B'_{1/3}B''_{2/3})\text{O}_3$  (where  $B' = \text{Zn}, \text{Mg}, \text{Co}, \text{Ni}$  and  $B'' = \text{Nb}, \text{Ta}$ ) general formula are extensively used in wireless communication technology, most notably as coupled resonators in cell phone band pass filters [1, 2]. For these applications, the dielectric resonators need to satisfy three important requirements; a large dielectric constant in the range from 20 to 50, a temperature coefficient of resonant frequency,  $\tau_f$ , near zero (i.e.  $|\tau_f| < 3$  ppm/K), and a quality factor,  $Q$  ( $= 1/\tan \delta$ ),

greater than 30,000 at 1 GHz. Any reduction in the loss tangent ( $\tan \delta$ ) results in a smaller insertion loss and sharper cut-offs in the microwave filter's characteristics [3]. In spite of the widespread utilization of high performance complex perovskite dielectrics in filter and other applications, a first-principles, quantitative understanding of microwave dielectric loss in these materials has not been fully developed.

Dielectric loss consists of intrinsic and extrinsic components. Since single phonon absorption processes does not satisfy the energy and momentum requirements, the intrinsic loss for practical dielectrics, including  $\text{Ba}(\text{Co}_{1/3}\text{Nb}_{2/3})\text{O}_3$ , was previously ascribed to two, three and higher order phonon absorption processes [4-6]. To mix the frequencies, non-linear components involving the anharmonic component of phonon modes are involved and these processes form the lower limit of the loss tangent, i.e., the loss tangent of an "ideal" crystal [6]. More recently, our group has conclusively shown that spin excitations in a material with a large fraction of magnetic elements such as Ni-doped  $\text{Ba}(\text{Zn}_{1/3}\text{Ta}_{2/3})\text{O}_3$  and Co-doped  $\text{Ba}(\text{Zn}_{1/3}\text{Nb}_{2/3})\text{O}_3$  dominate the intrinsic loss, at temperatures as high as  $\sim 250$  K [7, 8]. At room temperature, the losses in all practical materials are generally believe to arise from extrinsic factors associated with the presence of native and impurity point defects, pores, grain boundaries, and lattice strain [9-13]. With the goal of attaining the lowest loss tangent possible, the research and development community is pursuing methods to identify and eliminate these extrinsic sources during the synthesis of ceramic bodies.

It has been established that low dielectric loss occurs in dense and single phase  $\text{Ba}(\text{B}'_{1/3}\text{B}''_{2/3})\text{O}_3$  ceramics that possess high 1:2 ordering of  $B'$  and  $B''$  cations [14-17]. Although a first-principles model that accurately predicts loss based on the extent of ordering in the perovskites is not available, the correlation has been documented and attributed to a

significant reduction in nano-scale based anharmonicity in the phonons, resulting in decreased microwave loss [18-21]. A number of studies have observed an interesting phenomenon; small deviations from stoichiometry can increase the extent of cation ordering and reduce the loss tangent of these materials [22-25]. Consistent with such results, our recent study [26] found that the more strongly ordered Co-deficient ceramics with the compositions on the  $\text{Ba}_3\text{CoNb}_2\text{O}_9$ - $\text{Ba}_5\text{Nb}_4\text{O}_{15}$  joint had higher  $Q$ s than that of the stoichiometric  $\text{Ba}_3\text{CoNb}_2\text{O}_9$  ceramic. However, in contradiction to this trend, dense, single phase, and structurally 1:2 ordered Co-excessive ceramics with compositions on the  $\text{Ba}_3\text{CoNb}_2\text{O}_9$ - $\text{CoO}$  tie line had much lower  $Q$  values than those of the partially ordered stoichiometric ceramic. This was a clear sign that cation ordering alone is not a sufficient condition to achieve a minimum dielectric loss. This is not all that surprising since another extrinsic loss mechanism associated with a high defect density could be dominating the microwave properties. In one very interesting study of  $\text{Ba}(\text{Co}_{1/3}\text{Nb}_{2/3})\text{O}_3$  ceramics, Li et al. [27] reported that high-temperature sintering and subsequent slow cooling in flowing  $\text{O}_2$  atmosphere resulted in improved ordering, but increased the microwave loss due to the presence of hole type carrier conduction associated with the mixed presence of  $\text{Co}^{2+}$  and  $\text{Co}^{3+}$  on the B-site lattice.

In the present work, we study temperature and magnetic field dependence of dielectric loss of the Co-excessive, stoichiometric, and Co-deficient  $\text{Ba}(\text{Co}_{1/3}\text{Nb}_{2/3})\text{O}_3$  ceramics. We give strong evidence to show that in addition to microwave absorption from spin excitations of unpaired d-electrons of Co ions, polaron hopping between  $\text{Co}^{2+}$  and  $\text{Co}^{3+}$  cations also contributes to the dielectric loss in  $\text{Ba}(\text{Co}_{1/3}\text{Nb}_{2/3})\text{O}_3$  at cryogenic temperatures. Our work reported here involved suppressing the spin excitations with a large magnetic field in order to study two peaks in the loss tangent versus temperature relation at 25-30 K and 90 K, which were found to increase in magnitude with increasing Co content in the bulk dielectric

samples. Evidence that these peaks result from polaron hopping between  $\text{Co}^{2+}$  and  $\text{Co}^{3+}$  ions include the observations that their intensity (a) drops by about a factor of two in a large applied magnetic fields (5 T) and (b) correlates with both the fraction of the minority  $\text{Co}^{3+}$  in the dominant  $\text{Co}^{2+}$  matrix and D.C. conductivity at elevated temperatures. A magnetic-field independent high temperature peak at 250 K was found to dominate the room temperature microwave loss and its magnitude correlates with those of the low temperature peaks, which suggests that it could arise from free polaron hopping.

## II. Experimental Procedure

Ceramic samples with the target compositions of  $\text{Ba}_3\text{CoNb}_2\text{O}_9$  (stoichiometry),  $(1-x)\text{Ba}_3\text{CoNb}_2\text{O}_9-(x)\text{CoO}$  (Co excess) and  $(1-x)\text{Ba}_3\text{CoNb}_2\text{O}_9-(x)\text{Ba}_5\text{Nb}_4\text{O}_{15}$  (Co deficiency) where  $0.02 \leq x \leq 0.06$  were prepared by using conventional solid state method.  $\text{Co}_3\text{O}_4$  (Sigma-Aldrich, 99.9%),  $\text{Nb}_2\text{O}_5$  (Cerac, 99.99%) and  $\text{BaCO}_3$  (Alfa Aesar, 99.9%) were used as the raw materials and were mixed according to the desired stoichiometry by means of wet milling for 12 h in ethanol with yttrium-stabilized zirconia balls. The obtained slurry, then, was dried and calcined at 1150 °C for 5 h in air. The heated products were milled and dried again under the same condition that was described before. The prepared powders were employed to form cylindrical specimens with 2 cm diameter and 1 cm thickness under 115 MPa uniaxial pressure. Sintering was performed for the green ceramic pucks at 1400-1450 °C for 10 h in air with normal heating/cooling rates of 300 °C/h and 180 °C/h, respectively. After the sintering process, the top 2 mm of the sample surfaces was polished away to remove any surface contamination and non-stoichiometries. Ceramic samples with relative density of 98-99% were obtained. In order to exclude the effect of any secondary phases on the microwave dielectric properties of non-stoichiometric samples, we focused on the single phase, solid solution  $\text{Ba}_3\text{CoNb}_2\text{O}_9$ ,  $(1-x)\text{Ba}_3\text{CoNb}_2\text{O}_9-(x)\text{CoO}$  where  $x \leq 0.04$  and  $(1-x)\text{Ba}_3\text{CoNb}_2\text{O}_9-$

$(x)\text{Ba}_5\text{Nb}_4\text{O}_{15}$  ceramics where  $x \leq 0.02$  in this study. More detailed information about the  $\text{Ba}(\text{Co}_{1/3}\text{Nb}_{2/3})\text{O}_3$  sample preparation procedure and the chemical and structural properties of the samples are given in Reference [26].

For brevity in nomenclature, the stoichiometric  $\text{Ba}_3\text{CoNb}_2\text{O}_9$ , Co-excessive  $\text{Ba}_3\text{CoNb}_2\text{O}_9$   $[(1-x)\text{Ba}_3\text{CoNb}_2\text{O}_9-(x)\text{CoO}]$  and Co-deficient  $\text{Ba}_3\text{CoNb}_2\text{O}_9$   $[(1-x)\text{Ba}_3\text{CoNb}_2\text{O}_9-(x)\text{Ba}_5\text{Nb}_4\text{O}_{15}]$  ceramics are hereafter referred to as ST, CEx, and CDx, respectively, where  $x$  designates the degree of non-stoichiometry.

The microwave loss tangents of  $\text{Ba}(\text{Co}_{1/3}\text{Nb}_{2/3})\text{O}_3$  samples were measured using a dielectric resonator (DR) technique described in more detail in References [7] and [28].

Rectangular dielectric resonators with  $8.5 \text{ mm} \times 6.5 \text{ mm} \times 2 \text{ mm}$  dimensions were cut from as sintered ceramic pucks and then loaded into a  $20.3 \text{ mm} \times 6.1 \text{ mm} \times 15.2 \text{ mm}$  gold-plated copper cavity. The cavity was affixed to the end of a cryogenic dipping probe and subsequently inserted into a cryostat (PPMS, Model 6000, Quantum Design, San Diego, CA) for measurements at 2 K to 400 K in magnetic fields as high as 9 T. The microwave signals were transmitted and received through  $50 \Omega$  semi-rigid coaxial cables to and from the copper cavity. The distance between coupling loops and rectangular resonator was adjusted to be weakly coupled so that the unloaded  $Q$  is determined to better than a few percent. A HP8510C microwave Vector Network Analyzer (VNA) was used to measure  $S_{21}$  vector values. A LabVIEW program (National Instruments, Austin, TX) was used to control the cryostat temperature and magnetic field sequence and the VNA measurement routines. The recorded  $S_{21}$  values then were fitted to a circle in the Smith chart by using a Matlab script inserted into the LabVIEW computer module to determine the unloaded quality factor,  $Q$ . The values for the dielectric loss tangent, i.e.  $\tan \delta$ , were inferred from  $\tan \delta = 1/Q$ , such that

this value corresponds to an upper bound measurement value as a result of such additional contributions from coupling, near-field and radiation losses.

Magnetic susceptibility measurements were performed from 2–380 K in a magnetic field of 50 Oe using a Magnetic Property Measurement System (MPMS, Quantum Design) equipped with a superconducting quantum interference device.

The D.C. conductivity was measured in the temperature range from 423 K to 873 K on samples prepared with 5 mm diameter 100 nm thick Au contacts located on the top and bottom of a 2 mm thick sample using a picoammeter (HP4140b, Hewlett Packard, Palo Alto, CA) scanned between -2 V and 2 V.

### III. Results and Discussion

The temperature dependence of dielectric loss of CE0.04, ST, and CD0.02 ceramics are illustrated in Figs. 1(a)-(c). As can be observed, when the temperature drops from 300 K to 4 K, the dielectric loss under ambient condition increases monotonically in a Curie-type relation, indicating that microwave photon absorption tracks the population differences in the spin population and could thus be from an electron paramagnetic resonance process. Conclusive evidence that absorption from electron paramagnetic resonance spin excitations is the dominant loss mechanism at low temperatures is the strong reduction in the loss tangent when a 5 T field is applied, also shown in Fig. 1. Our earlier publications have shown that the same process also dominates the microwave loss at cryogenic temperatures for a number of other transition-metal-doped materials, including Ni-doped  $\text{Ba}(\text{Zn}_{1/3}\text{Ta}_{2/3})\text{O}_3$ , Co-doped  $\text{Ba}(\text{Zn}_{1/3}\text{Nb}_{2/3})\text{O}_3$ , Cu, Mn, Fe-doped  $\text{ZrTiO}_4\text{-ZnNb}_2\text{O}_6$ , and Cu, Mn, Fe-doped  $\text{BaTi}_4\text{O}_9\text{-BaZn}_2\text{Ti}_4\text{O}_{11}$  [7-9]. Other loss mechanisms such as phonon absorption or carrier transport

would not be expected to have such a strong field dependence. Also note that the field dependence of the loss tangent is very small above ~175-200 K, indicating that electron paramagnetic absorption does not dominate loss at elevated temperatures.

Fig. 2 reveals a representative example of the loss tangent as a function of magnetic field at both 20 K and room temperature (300 K). The loss measured at 20 K for the CD0.02 sample exhibits a strong and dipole broadened electron paramagnetic resonance (EPR) signal at 1945 G field, which dominates the dielectric loss even down to zero applied fields. This peak's Lande g-factor calculated from  $h\nu = \mu_B g B_{ex}$  is 3.88, a value characteristic of paramagnetic  $\text{Co}^{2+}$  cations.  $h$  is Plank constant,  $\nu = 10.4$  GHz is the resonant frequency of the CD0.02 sample,  $\mu_B$  is the Bohr magneton, and  $B_{ex}$  is applied magnetic field. Similar EPR spectra are obtained for the other samples. The 300 K microwave loss is not magnetic field dependent and thus does not exhibit any discernable EPR features, presumably due to the very short spin excitation lifetime at this temperature.

Based on the width of the peak in the 20 K spectra, the paramagnetic resonance signal arises from super-exchange coupled  $\text{Co}^{2+}$  ions [7-9]. Such a broad peak is distinctly different from the sharp peaks found in isolated  $\text{Co}^{2+}$  point defect spectra found in dilutely-doped material [29]. The dipole broadened peaks observed in our study are characteristic of EPR absorption involving spin excitations of electrons involving multiple super-exchange coupled  $\text{Co}^{2+}$  ions. The large broadening can be attributed to the fact that when  $\text{Co}^{2+}$  ions are separated by a distance less than  $a/2$ , they form super-exchange coupled spin clusters [30]. Our earlier X-ray diffraction Rietveld refinement analysis showed that the CD0.02 sample has a trigonally 1:2 ordered perovskite structure ( $P\bar{3}m1$  space group) with  $\text{Co}^{2+}$  and  $\text{Nb}^{5+}$  cations



occupying 1b and 2d Wyckoff sites [26]. In this arrangement, the distance between  $\text{Co}^{2+}$  cations was calculated to be  $5.2(2)$  Å, indicating that super-exchange-coupled clusters would be expected to form. These results are very similar to that found in the study reported by Liu et al. [7] on Co-doped commercial  $\text{Ba}(\text{Zn}_{1/3}\text{Nb}_{2/3})\text{O}_3$  and Zhang et al. [8] on  $\text{Ba}(\text{Zn}_{1/3}\text{Nb}_{2/3})\text{O}_3$  made in our laboratory with a range of Co-content.

To study the extrinsic dielectric loss mechanisms, we now focus on the temperature-dependence of loss with the spin-loss suppressed, i.e. in the presence of a 5 T applied magnetic field, as illustrated in the insets of Figs. 1(a)-(c) and Fig. 3(a). The quality factor of CD0.02 was also measured at even a higher applied magnetic field of 9 T and the results were not significantly different. We can conclude that 5 T field is sufficient to completely remove the spin-related source of loss over the entire temperature range. It is observed from Fig. 3(a) that two low temperature loss peaks occur at 25-30 K and 90 K in the loss tangent versus temperature measurements. Interestingly, when moving from Co-rich sample (CE0.04) toward Co-deficient ceramic (CD0.02) (see Fig. 3(b)), the intensity of the dielectric loss peaks decreases.

In our analysis of the loss tangent of  $\text{Ba}(\text{Co}_{1/3}\text{Nb}_{2/3})\text{O}_3$  ceramics measured at 5 T, the intrinsic dielectric loss is first subtracted from the experimental loss tangent curves and then they are fitted with two low temperature Debye-type loss peaks at 25-30 K and 90 K and an additional high temperature Debye-type peak centered at ~250 K, using the Debye model equation and the associated thermally activated relaxation time  $\tau$  [31]

$$\tan\delta(\omega, T) = \frac{\eta N_d P^2}{\epsilon_r \epsilon_0 k_B T} \frac{\omega \tau}{1 + \omega^2 \tau^2} \quad (1)$$

$$\tau = \tau_0 \exp\left(\frac{W}{k_B T}\right) \quad (2)$$

where  $T$  is the temperature,  $k_B$  is the Boltzmann constant,  $\omega$  is the angular microwave frequency,  $\eta$  is the field correction factor of the order of one,  $N_d$  corresponds to the concentration of electric dipoles with moment  $P$ , assumed to be  $1.6 \times 10^{-29}$  C.cm,  $W$  is the activation energy,  $\tau_0$  is the pre-exponential factor of the relaxation time. During the fitting process,  $N_d$ ,  $\tau_0$ , and  $W$  were taken as fitting parameters and relaxed to achieve the best convergence. To evaluate the background from the intrinsic loss due to two phonon process (intrinsic loss), we used the model relation of Sparks, King, and Mills based on the methodology developed by Zuccaro [32].

The results of the analysis for the CE0.04, ST, and CD0.02 ceramics are shown in Fig.

4. Agreement between the fit and measured data is quite good. The values of the obtained fitting parameters  $N_d$ ,  $\tau_0$ , and  $W$  together with temperatures corresponding to the maximum of the three peaks ( $T_{\max}$ ) and extent of contribution of each dipole relaxation to dielectric constant ( $\Delta\epsilon$ ) are listed for CE0.04 and CD0.02 samples in Table 1. Peak 1, Peak 2, and Peak 3 are centered at 25-30 K, 90 K, and 250 K with activation energies ( $W$ ) in the range of 2.1-6.3 meV, 32.0-40.1 meV, and 61.0-63.3 meV, respectively. More importantly, the total dipole density resulted from these three loss peaks was found to be  $1.22 \times 10^{18} \text{ cm}^{-3}$  for Co-excessive ceramic (CE0.04), while it decreased to  $3.96 \times 10^{17} \text{ cm}^{-3}$  for Co-deficient sample (CD0.02). Thus, we find that by changing the stoichiometry of  $\text{Ba}(\text{Co}_{1/3}\text{Nb}_{2/3})\text{O}_3$  compounds from Co rich compositions towards Co poor compositions, as delineated in the ternary phase diagram (Fig. 3(b)), the magnitude of all 3 peaks is markedly decreased. It is also worth noting that the high temperature peak with a maximum at 250 K (Peak 3) dominates the room temperature dielectric loss.

We next discuss the potential causes for the dielectric loss peaks. Microwave loss can be caused by a number of mechanisms that can be fit to Debye model equations. It can arise from ions or carriers moving from one low-energy position over a barrier to another position within a single lattice site or it can arise from them moving from one localized lattice site over a barrier to another site. For charge carrier transport, the latter case is often labeled hopping conduction and can involve electrons or holes that are undressed (i.e. variable range or free carrier hopping) or dressed by lattice relaxation (i.e. polaron conduction) [33, 34]. By considering the related literature, it is found that some authors have used activation energy ( $W$ ) and/or relaxation time ( $\tau_0$ ) to distinguish the polaron hopping mechanism from localized ionic motion mechanism. As an example, Zuccaro et al. [32] observed a Debye-type dielectric loss peak at about 70 K in  $\tan \delta(T)$  of single crystal  $\text{LaAlO}_3$ . They attributed the loss peak to the local motions of impurity ions between equilibrium interstitial positions of the same lattice site due to the calculated low activation energy of 31 meV and the relaxation time in the order of  $10^{-13}$  s, corresponding to near the expected frequency of the optical phonon at the Brillion zone center. Breeze et al. [35] also reported a small activation energy (<20 meV) for the collective motion of ions responsible for the observed Debye type loss in the case of MgO bi-crystal containing a single grain boundary. On the other hand, similar to ionic motion, electron or polaron hopping from site to site could possess activation energy in a range of  $\mu\text{eV}$  to several eV. Thus, since a detailed quantitative microscopic understanding of the electron and ion motion in these materials is not known, it is not possible to confidently reach a strong conclusion about the physical nature of the observed loss peaks through the evaluation of the activation energy and relaxation times alone. Instead, we will explore other ways to discern the physical origin of Debye peaks measured in the stoichiometric and non-stoichiometric  $\text{Ba}(\text{Co}_{1/3}\text{Nb}_{2/3})\text{O}_3$ .

We will focus on the magnetic and temperature dependence features of loss tangent data to discover useful information about the observed loss peaks. When the loss tangent values measured at 5 T are subtracted from those of measured in the absence of a magnetic field, then  $\Delta \tan \delta = \tan \delta(\text{at } 0 \text{ T}) - \tan \delta(\text{at } 5 \text{ T})$  shows the loss originated from the magnetic dependent sources, as illustrated in Fig. 1(d) for CD0.02 sample.

The  $\Delta \tan \delta$  curve is fitted by summing a Curie-Weiss type relation,  $\tan \delta = \frac{a}{T-c} + b$ , for the spin excitations, where  $a$ ,  $b$ , and  $c$  are fitting parameters and two low temperature Gaussian peaks, named as Peak 1 and Peak 2 located at  $\sim 30$  K and  $\sim 90$  K, respectively, as shown in Fig. 1(d). The presence of Peak 1 and Peak 2 in the  $\Delta \tan \delta$  data indicates that the observed low temperature peaks are affected by the presence of the high 5 T external magnetic field. When the values for the intensity of the peaks measured without an applied field were directly compared to the measurements made at 5 T, it was found the intensities of Peak 1 and Peak 2 decrease by a factor of  $\sim 2$  after the application of a field, while the high temperature Peak 3 located above 200 K does not significantly change. Magnetic-field dependent transport has also been found in oxides with mixed-valence magnetic impurities )i.e.  $\text{La}_{1.2}\text{Sr}_{1.8}\text{Mn}_2\text{O}_7$  [36],  $\text{NiO}$  [37] and  $\text{Mn}_{0.6}\text{Zn}_{0.4}\text{Fe}_2\text{O}_4$  [38]( and the reduction in the conduction in field was attributed to a magnetic-field dependent carrier hopping process in which the potential number of sites diminished when the spin population became more strongly polarized in the field.

Next, we consider the mechanism responsible for the formation of polarons and their concentration variations as a function of composition in the  $\text{Ba}(\text{Co}_{1/3}\text{Nb}_{2/3})\text{O}_3$  based ceramics. For this purpose, the magnetic susceptibility of samples was measured in the temperature range of 2–380 K. Fig. 5(a) presents the temperature dependence of molar magnetic

susceptibility ( $\chi_{mol}$ ) normalized for 1 mole Co concentration of Co-excessive (CE0.04), stoichiometric (ST), and Co-deficient Ba(Co<sub>1/3</sub>Nb<sub>2/3</sub>)O<sub>3</sub> (CD0.02) ceramics. The variation of  $\chi_{mol}$  with temperature resembles the modified Curie–Weiss law at low temperature

$$\chi_{mol} = \frac{C}{T - \theta_w} + \chi_0 \quad (3)$$

where  $C$  is the Curie constant,  $\theta_w$  defines the paramagnetic Weiss temperature and  $\chi_0$  shows temperature independent term. The inset in Fig. 5(a) gives a magnified view of a part of magnetic susceptibility curves. Although,  $\chi_{mol}$  is normalized for 1 mole Co and therefore identical curves should result, it is clearly observed that  $\chi_{mol}$  possesses higher value by deviation from Co-rich sample (CE0.04) towards Co-poor sample (CD0.02). The grey region depicted in the inset of Fig. 5(a) reveals the observed difference in molar magnetic susceptibility of CE0.04 (lower boundary) and CD0.02 (upper boundary) where the curve belonged to ST ceramic is located within this region.

The Co<sup>2+</sup> in the high spin state has a <sup>4</sup>T<sub>1</sub> ground term and effective magnetic moment,  $\bar{\mu}$ , in Bohr magnetons  $\mu_B$  is given by [39]

$$\bar{\mu}^2 = \frac{3[3 \cdot 15x + 3 \cdot 92 + (2 \cdot 84x + 2 \cdot 13) \exp\left(-\frac{15x}{4}\right) + (4 \cdot 7x - 6 \cdot 05) \exp(-6x)]}{x[3 + 2 \exp\left(-\frac{15x}{4}\right) + \exp(-6x)]} \quad (4)$$

where  $x = \frac{\lambda}{k_B T}$  and  $\lambda = -170 \text{ cm}^{-1}$  is the spin-orbit coupling constant. The effective magnetic moment,  $\bar{\mu}$ , is related to the Curie constant  $C$  by the following equation

$$C = \frac{N_A \bar{\mu}^2 \mu_B^2}{3k_B} \quad (5)$$

where  $N_A$  is Avogadro's number. The measured  $\frac{1}{\chi_{mol}}$  versus temperature curves were fitted by equations (3) to (5) as shown in Fig. 5(b) and (c) for CE0.04 and CD0.02 ceramics, respectively. The  $N_A$ ,  $\theta_w$ , and  $\chi_0$  were taken as fitting parameters and relaxed during fitting

process. Note that the  $\frac{1}{\chi_{mol}}$  versus temperature curve intersects the ordinate at  $\sim 0$  K, indicating that the sample is paramagnetic at all temperatures.

If all the incorporated Co ions were in the paramagnetic state  $\text{Co}^{2+}$  then the fitting parameter  $N_A$  would equal Avogadro's number,  $6.022 \times 10^{23} \text{ mol}^{-1}$ . The decrease of  $\chi_{mol}$  as one goes from Co-deficient to Co-excessive compositions indicates that the greater the Co content, the smaller the fraction of Co ions are in the paramagnetic  $\text{Co}^{2+}$  state. The rest are in a diamagnetic state, presumably the low spin state  $\text{Co}^{3+} d^6$  cations [29]. No evidence of metallic Co or other phases were detected in the X-ray analysis. The fraction of  $\text{Co}^{2+}$  and  $\text{Co}^{3+}$  cations that we infer from the fit indicates that nearly all of the cobalt ions are in the form of paramagnetic  $\text{Co}^{2+}$  for CD0.02 composition (i.e. up to 0.5%  $\text{Co}^{3+}$  ions), while in the stoichiometric ST and CE0.04 ceramics there are  $1.4 \pm 0.5\%$  and  $8.7 \pm 0.5\%$   $\text{Co}^{3+}$  of the total cobalt ions, respectively, as given in Fig. 5(d). The presence of predominantly  $\text{Co}^{2+}$  and up to  $\sim 9\%$   $\text{Co}^{3+}$  suggests that the observed polaron hopping occurs by electron transfer from a  $\text{Co}^{2+}$  site to an acceptor  $\text{Co}^{3+}$  site. Polaron hopping of holes between the  $\text{Co}^{3+}$  and  $\text{Co}^{2+}$  has also been reported in a number of other oxide material systems [33, 34].

Fig. 6(a) illustrates the D.C. conductivity as a function of temperature. Activation energies of CE0.04, ST, and CD0.02 samples are found to be 0.82-0.89 eV, an activation energy that falls in the range of free polarons [33, 34]. Also, the measured conductivities are highest in the Co excessive sample (CE0.04), are lower in the stoichiometric sample (ST), and are the lowest in the Co deficient sample (CD0.02). We find a strong correlation between the measured D.C. conductivity at 873 K, the fraction of  $\text{Co}^{3+}$  present in the lattice, the intensity of Peak 1 and Peak 2 (Fig. 6(b)), and the room temperature loss tangent (Fig. 6(c)). Since the measured D.C. carrier conduction has an activation energy that falls in the range of

free polarons, we suggest that microwave absorption by free polaron hopping could play a dominant role in establishing the loss tangent at room temperature. This explanation is in agreement with that proposed by Li et al. [27], who demonstrated significant influence of the extrinsic electrical conduction associated with the presence of mixed  $\text{Co}^{2+}$  and  $\text{Co}^{3+}$  cations on the room temperature dielectric loss of dense, single phase, and ordered  $\text{Ba}(\text{Co}_{1/3}\text{Nb}_{2/3})\text{O}_3$  ceramics. This will be discussed in more detail later in this section. We can now rule out free carrier conduction as a significant loss source at room temperature, since if we extrapolate the D.C. conductivity of sample CD0.02 at room temperature (i.e.  $10^{-13}$  S/m) and assume that it is not frequency dependent, a loss tangent of  $6 \times 10^{-15}$  is inferred from Maxwell's equations ( $\tan \delta = \frac{\sigma}{\omega \epsilon \epsilon_0}$ ). This value is significantly smaller than the measured room temperature microwave loss tangent ( $1.8 \times 10^{-4}$ ).

Some insight into the polaron properties can be gained from analysis of the high temperature transport data and the Mott polaron model [40, 41]. The activation energy for hopping ( $W$ ) depends upon the energy from the screened potential ( $W_H$ ) required to move from site to site and a disorder energy ( $W_D$ ) that results from the random potential associated with the compensating background donor defects that are responsible for generating  $\text{Co}^{3+}$  sites. For the Co-excess compound with a fraction of 8.7%  $\text{Co}^{3+}$ , we can infer the polaron radius,  $r_0$ , to be 3.7 Å from the measured activation energy of 0.85 eV and the relation:

$$W = W_H + \frac{1}{2}W_D = \frac{1}{4} \frac{e^2}{\epsilon_0} \left( \frac{1}{\epsilon_\infty} - \frac{1}{\epsilon} \right) \left( \frac{1}{r_0} - \frac{1}{R} \right) + \frac{1}{2}W_D \quad (6)$$

where  $W_D|_{8.7\% \text{ donors}} \sim C e^2 / \epsilon \epsilon_0 R_{\text{donor}} = 0.18 \text{ eV}$  and  $e$  is the charge on the electron,  $\epsilon$  and  $\epsilon_\infty$  are the static (32.13), high frequency (4.6) dielectric constant, respectively,  $\epsilon_0$  corresponds to the vacuum permittivity ( $8.85 \times 10^{-12}$  F/m),  $R_{\text{donor}}$  (13.9 Å) is the mean distance of the donor concentration ( $4.3 \times 10^{20}/\text{cm}^3$ ),  $C$  is the prefactor that depends on the fraction of donors and is

0.45 for 8.7% of donors [42], and  $R$  is the distance between Co sites on the  $\text{Ba}(\text{Co}_{1/3}\text{Nb}_{2/3})\text{O}_3$  lattice (5.8 Å). The polaron radius is significantly smaller than the distance between Co lattice sites, consistent with it being a small polaron. From these calculations, we can infer the tunneling probability,  $\alpha$  to be  $2.96 \text{ m}^{-1}$  by fitting relation (7) to our data.

$$\sigma = c(1 - c)(\nu_0 N e^2 R^2 / k_B T) \exp(-2\alpha R) \exp(-(W_H + \frac{1}{2}W_D)/k_B T) \quad (7)$$

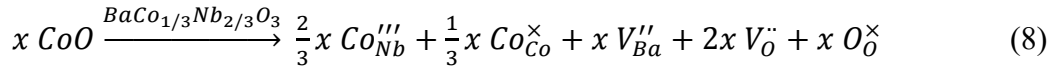
where  $N$  is the number of  $\text{Co}^{3+}$  sites ( $4.3 \times 10^{20}/\text{cm}^3$ ),  $\nu_0$  is the jump frequency (longitudinal optical phonon rate of  $\sim 10^{13}/\text{s}$ ), and  $c$  is the ratio of  $\text{Co}^{3+}$ :total Co lattice sites. This value for the tunneling probability and all values that we have calculated for the polar conduction are physically reasonable and consistent with that observed for the peaks in the loss tangent at cryogenic temperatures and for the high temperature conduction.

To delineate the type of polaron hopping, we can compare the results of the analysis summarized in Table 1 and compare it to typical hopping times. For adiabatic hopping, the chances of a hop taking place is near unity, which typically falls near the longitudinal optical phonon frequency of  $\sim 10^{13}/\text{s}$ , whereas for non-adiabatic hopping the chances are much less and the hopping times are therefore much longer than the attempt frequency. From the analysis presented in Table 1, Peak 1 could be tentatively assigned to non-adiabatic hopping, while Peak 2 and Peak 3 could be assigned to adiabatic hopping.

To understand the mechanism responsible for the variation of the oxidation state of  $\text{Co}^{2+}$  to  $\text{Co}^{3+}$ , point defect chemistry of Co-excessive  $\text{Ba}(\text{Co}_{1/3}\text{Nb}_{2/3})\text{O}_3$  compositions is considered. These compositions are located on the  $\text{Ba}_3\text{CoNb}_2\text{O}_9$ - $\text{CoO}$  tie line in the ternary  $\text{BaO}$ - $\text{CoO}$ - $\text{Nb}_2\text{O}_5$  phase diagram and form single phase  $\text{Ba}(\text{Co}_{1/3}\text{Nb}_{2/3})\text{O}_3$  solid solutions when  $x \leq 0.04$  in  $(1-x)\text{Ba}_3\text{CoNb}_2\text{O}_9$ - $x\text{CoO}$  compositions. Accommodation of Co excess in the  $\text{Ba}(\text{Co}_{1/3}\text{Nb}_{2/3})\text{O}_3$  crystal structure could be described according to the following mechanisms:

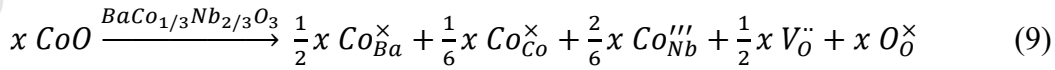


(i) Substitution of excessive Co cations into Nb sites ( $Co'''_{Nb}$ ) and formation of Ba and oxygen vacancies, i.e.,  $V''_O$  and  $V''_{Ba}$  according to the below reaction



In this case, charge compensation of  $Co'''_{Nb}$  and  $V''_{Ba}$  defects is reached by the formation of  $V''_O$ .

(ii) There is another possibility that the excess Co is simultaneously accommodated in the Ba and Nb vacant sites and causes  $Co^\times_{Ba}$  and  $Co'''_{Nb}$  defects



According to the second mechanism,  $Co^\times_{Ba}$ ,  $Co'''_{Nb}$  defects and oxygen vacancy  $V''_O$  could be present in the Co-rich  $Ba(Co_{1/3}Nb_{2/3})O_3$  ceramics. Substitution of excess Mg cations into Ba sites was reported by Kolodiaznyi [43] for the Mg-rich  $Ba(Mg_{1/3}Ta_{2/3})O_3$  ceramics.

Although, the low frequency dielectric spectroscopy showed that  $Mg^\times_{Ba}$  could be dominant point defect in the solid solution located on the  $Ba_3MgTa_2O_9$ - $Mg_4Ta_2O_9$  joint, similar investigations (not given here) of  $Ba(Co_{1/3}Nb_{2/3})O_3$  ceramics did not demonstrate the existence of  $Co^\times_{Ba}$  point defects in a large quantity for  $Ba_3CoNb_2O_9$ - $CoO$  compositions. It is also expected in reaction (8) that some part of the charge compensation for  $Co'''_{Nb}$  and  $V''_{Ba}$  could be reached by changing the oxidation state of  $Co^{2+}$  to  $Co^{3+}$ , i.e., the formation of  $Co^\times_{Co}$  point defects with positive charge. This process is a common type of charge compensation in acceptor-doped  $CoO$  ceramics. For example, it is believed that monovalent Li cations substituted for divalent Co ions would be charge compensated by the presence of trivalent Co cations, which leads to mixed-valent  $CoO$  compound. On the other hand, our previous point defect study of Co-deficient compositions located on the  $Ba_3CoNb_2O_9$ - $Ba_5Nb_4O_{15}$  tie line demonstrated that the point defect chemistry of these solid solutions could be explained reasonably well by the formation of dominant  $Ba^\times_{Co}$  defects and all the oxygen sites would be filled without any  $V''_O$  existence [26]. Alternatively, the compositions along the  $Ba_3CoNb_2O_9$ -

$x\text{Ba}_5\text{Nb}_4\text{O}_{15}$  tie line can be represented by the Co-site accommodating Co vacancies and excess Nb:  $\text{Ba}(\text{Co}_{1-x}\text{V}_{\text{Co}3x/5}\text{Nb}_{2x/5})_{1/3}\text{Nb}_{2/3}\text{O}_3$  [23]. The latter scenario, however, was ruled out in Ref. [26] based on the unit cell volume expansion with an increase in  $x$ . Therefore, from the above discussion, we suggest that the deviation in stoichiometry as one goes from the Co-deficient to Co-excessive regions, the major point defect type would change from  $\text{Ba}_{\text{Co}}^{\times}$  to the positive  $V_{\text{O}}^{\bullet}$  and  $\text{Co}_{\text{Co}}^{\bullet}$  and negative  $V_{\text{Ba}}^{\prime\prime}$ , and  $\text{Co}_{\text{Nb}}^{\prime\prime\prime}$  defects, respectively.

The presence of mixed valences of transition metal ions like cobalt cations  $\text{Co}^{2+}$  and  $\text{Co}^{3+}$  would facilitate polaron hopping, as discussed earlier in this work and in the literature [33, 34, 44]. At low temperatures these holes are most likely bound to the lattice defects, such as  $\text{Co}_{\text{Nb}}^{\prime\prime\prime}$  and  $V_{\text{Ba}}^{\prime\prime}$  centers in  $\text{Ba}(\text{Co}_{1/3}\text{Nb}_{2/3})\text{O}_3$  ceramics. The low temperature peaks at 25-30 K and 90 K observed in  $\tan \delta(T)$  curves in Fig. could thus be attributed to bound polaron hopping.

We speculate that Peak 1, with very small activation energy of 2.1-6.3 meV, is tentatively attributed to polaron hopping of  $V_{\text{Ba}}^{\prime\prime}$ -bound holes between  $\text{Co}^{2+}$  and  $\text{Co}^{3+}$  sites. Then, we suggest that Peak 2 could arise from hopping of  $\text{Co}_{\text{Nb}}^{\prime\prime\prime}$ -bound holes from one  $\text{Co}^{3+}$  ion to its neighbor  $\text{Co}^{2+}$  ion, with presumably a higher energy barrier of 32.0 - 40.1 meV. The higher intensities of Peak 1 and Peak 2 for Co-rich samples than those of Co-deficient ones are ascribed to the formation of  $\text{Co}_{\text{Co}}^{\bullet}$  defects in the crystal lattice by deviation of the compositions from Co-deficient toward Co excessive region.

#### IV. Conclusion

Spin excitation of unpaired d electrons of Co ions in  $\text{Ba}(\text{Co}_{1/3}\text{Nb}_{2/3})\text{O}_3$  ceramics dominate microwave loss at cryogenic temperatures. Three additional peaks were detected in the  $\tan \delta(T)$  curves and were modeled based on Debye type relation. The loss associated with these three peaks became progressively smaller as one goes from Co-excessive to Co-deficient

Ba(Co<sub>1/3</sub>Nb<sub>2/3</sub>)O<sub>3</sub> compositions. The two low temperature peaks located at 25-30 K and 90 K possessed 2.1-6.3 meV and 32.0-40.1 meV activation energy and were attributed to bound polaron hopping of holes. The third peak maximized at 250 K with 61.0-63.3 meV activation energy, directly affects room temperature dielectric loss and shows that defects responsible for carrier conduction play an important role in establishing the loss tangent at room temperature. We have speculated that it could result from free polaron transport, although additional work needs to be done to validate this conclusion.

### Acknowledgements

The collaboration between Dr. T. Kolodiaznyi (NIMS) and Prof. N. Newman (ASU) was partially supported by Grant-in-Aid for Scientific Research 26400323 from JSPS. The authors are also very grateful to Prof. David Ferry for reviewing the manuscript and his very valuable suggestions.

### References

1. Cava RJ. Dielectric materials for applications in microwave communications. *J Mater Chem.* 2001;11:54-62.
2. Fiedziuszko SJ, Hunter IC, Itoh T, et al. Dielectric materials, devices, and circuits. *IEEE Trans. Microwave Theory Technol.* 2002;50:706-720.
3. Reaney IM, Iddles D. Microwave dielectric ceramics for resonators and filters in mobile phone networks. *J Am Ceram Soc.* 2006;89:2063-2072.
4. Wu EJ, Ceder G. Computational investigation of dielectric absorption at microwave frequencies in binary oxides. *J Appl Phys.* 2001;89:5630-5636.

5. Shtin NA, Romero JML, Prokhorov E, Theory of fundamental microwave absorption in sapphire ( $\alpha$ -Al<sub>2</sub>O<sub>3</sub>). *J Appl Phys*. 2009;106:104115.
6. Gurevich V, Tagantsev A. Intrinsic dielectric loss in crystals. *Adv Phys*. 1991;40:719-767.
7. Liu L, Matusevich A, Garg C, et al. The dominance of paramagnetic loss in microwave dielectric ceramics at cryogenic temperatures. *Appl Phys Lett*. 2012;101:252901.
8. Zhang S, Devonport A, Newman N. Main Source of microwave loss in transition-metal-doped Ba(Zn<sub>1/3</sub>Ta<sub>2/3</sub>)O<sub>3</sub> and Ba(Zn<sub>1/3</sub>Nb<sub>2/3</sub>)O<sub>3</sub> at cryogenic temperatures. *J Am Ceram Soc*. 2015;98:1188-1194.
9. Liu L, Flores M, Newman N. Microwave loss in the high-performance dielectric Ba(Zn<sub>1/3</sub>Ta<sub>2/3</sub>)O<sub>3</sub> at 4.2 K. *Phys Rev Lett*. 2012;109:257601.
10. Pullar RC, Penn SJ, Wang X, et al. Dielectric loss caused by oxygen vacancies in titania ceramics. *J Eur Ceram Soc*. 2009;29:419-424.
11. Templeton A, Wang X, Penn SJ, et al. Microwave dielectric loss of titanium oxide. *J Am Ceram Soc*. 2000;83:95-100.
12. Penn SJ, Alford NMN, Templeton A, et al. Effect of porosity and grain size on the microwave dielectric properties of sintered alumina. *J Am Ceram Soc*. 1997;80:1885-1888.
13. Rong G, Newman N, Shaw B, et al. Role of Ni and Zr doping on the electrical, optical, magnetic, and structural properties of barium zinc tantalate ceramics. *J Mater Res*. 1999;14:4011-4019.
14. Matsumoto K, Hiuga T, Takada K, et al. Ba(Mg<sub>1/3</sub>Ta<sub>2/3</sub>)O<sub>3</sub> ceramics with ultra-low loss at microwave frequencies. *Sixth IEEE International Symposium on Applications of Ferroelectrics*. 1986:8-21.
15. Davies P, Wu H, Borisevich AY, et al. Crystal chemistry of complex perovskites: new cation-ordered dielectric oxides. *Annu Rev Mater Res*. 2008;38:369-401.

16. Desu S, O'Bryan HM. Microwave loss quality of  $\text{BaZn}_{1/3}\text{Ta}_{2/3}\text{O}_3$  ceramics. *J Am Ceram Soc.* 1985;68:546-551.
17. Reaney IM, Wise PL, Qazi I, et al. Ordering and quality factor in  $0.95\text{BaZn}_{1/3}\text{Ta}_{2/3}\text{O}_3$ – $0.05\text{SrGa}_{1/2}\text{Ta}_{1/2}\text{O}_3$  production resonators. *J Eur Ceram Soc.* 2003;23:3021-3034.
18. Kawashima S, Nishida M, Ueda T, et al.  $\text{BaZn}_{1/3}\text{Ta}_{2/3}\text{O}_3$  ceramics with low dielectric loss at microwave frequencies. *J Am Ceram Soc.* 1983;66:421–423.
19. Petzelt J, Setter N. Far infrared spectroscopy and origin of microwave losses in low-loss ceramics. *Ferroelectrics.* 1993;150:89–102.
20. Petzelt J, Kamba S, Kozlov GV, et al. Dielectric properties of microwave ceramics investigated by infrared and submillimeter spectroscopy. *Ferroelectrics.* 1996;176:145–65.
21. Davies PK, Jianzhu T, Taki N. Effect of ordering-induced domain boundaries on low-loss  $\text{Ba}(\text{Zn}_{1/3}\text{Ta}_{2/3})\text{O}_3$ – $\text{BaZrO}_3$  perovskite microwave dielectrics. *J Am Ceram Soc.* 1997;80:1727-1740.
22. Surendran KP, Sebastian MT, Mohanan P, et al. Effect of nonstoichiometry on the structure and microwave dielectric properties of  $\text{Ba}(\text{Mg}_{0.33}\text{Ta}_{0.67})\text{O}_3$ . *Chem Mater.* 2005;17:142–151.
23. Wu H, Davies PK. Influence of non-stoichiometry on the structure and properties of  $\text{Ba}(\text{Zn}_{1/3}\text{Nb}_{2/3})\text{O}_3$  microwave dielectrics: II. compositional variations in pure BZN. *J Am Ceram Soc.* 2006;89:2250-2263.
24. Ohsato H, Koga E, Kagomiya I, et al. Dense composition with high Q on the complex perovskite compounds. *Ferroelectrics.* 2009;387:28-35.
25. Koga E, Yamagishi Y, Moriwake H, et al. Large Q factor variation within dense, highly ordered  $\text{Ba}(\text{Zn}_{1/3}\text{Ta}_{2/3})\text{O}_3$  system. *J Eur Ceram Soc.* 2006;26:1961-1964.

26. Sayyadi-Shahraki A, Taheri-Nassaj E, Gonzales J, et al. Effect of non-stoichiometry on the densification, phase purity, microstructure, crystal structure, and dielectric loss of Ba(Co<sub>1/3</sub>Nb<sub>2/3</sub>)O<sub>3</sub> ceramics. *J Eur Ceram Soc*. 2017;37:3335-3346.
27. Li M, Feteira A, Mirsaneh M, et al. Influence of nonstoichiometry on extrinsic electrical conduction and microwave dielectric loss of BaCo<sub>1/3</sub>Nb<sub>2/3</sub>O<sub>3</sub> ceramics. *J Am Ceram Soc*. 2010;93:4087-4095.
28. Newman N, Liu L, Hanley R, et al. Resonator techniques to characterize material and device properties at microwave frequencies in the quantum design PPMS measurement system. *Application Note*. 2013;40:1084-750.
29. Langhammer H, Böttcher R, Müller T, et al. Defect properties of cobalt-doped hexagonal barium titanate ceramics. *J Phys: Condense Matter*. 2015;27:295901.
30. Che M, Djéga-Mariadassou G, Dyrek K, et al. An EPR investigation of Co<sup>2+</sup> in CoO—ZnO textured powders. *Zeitschrift für Physikalische Chemie*. 1987;152:131-138.
31. Bunget I, Popescu M. Physics of Solid Dielectrics, Material Science Monograph 19. Elsevier, Amsterdam, 1984.
32. Zuccaro C, Winter M, Klein N, et al. Microwave absorption in single crystals of lanthanum aluminate. *J Appl Phys*. 1997;82:5695-5704.
33. Bosman A, Crevecoeur C. Dipole relaxation losses in CoO doped with Li or Na. *J Phys Chem Solids*, 1968;29:109-113.
34. Iguchi E, Hashimoto T, Yokoyama S. Electrical transports and stability of small polarons of O 2<sub>p</sub> holes in Li<sub>x</sub>Co<sub>1-x</sub>O. *J Phys Soc Jpn*. 1996;65:221-229.
35. Breeze JD, Perkins JM, McComb DW, et al. Do grain boundaries affect microwave dielectric loss in oxides?. *J Am Ceram Soc*. 2009;92:671-674.
36. Chen XJ, Zhang CL, Almasan CC, et al. Small-polaron hopping conduction in bilayer manganite La<sub>1.2</sub>Sr<sub>1.8</sub>Mn<sub>2</sub>O<sub>7</sub>. *Phys Rev B*. 2003;67:094426.

37. Keem J, Honig J, Van Zandt LL. Localized charge carrier transport in pure single crystals of NiO. *Philos Mag B*. 1978;37:537-543.
38. El-Sayed H, Effect of magnetic field on the formation of spin-polaron in Mn-Zn ferrites. *Am J Appl Sci*. 2006;3:2033-2036.
39. Mabbs FE, Machin DJ. Magnetism and transition metal complexes. Dover Publications. 2008:87-90.
40. Mott N. Conduction in glasses containing transition metal ions. *J Non-Cryst Solids*. 1968;1:1-17.
41. Austin I, Mott N.F. Polarons in crystalline and non-crystalline materials. *Adv Phys*. 1969;18: 41-102.
42. Miller A, Abrahams E. Impurity conduction at low concentrations. *Phys Rev*. 1960;120:745-755.
43. Kolodiazhnyi T. Origin of extrinsic dielectric loss in 1:2 ordered, single-phase BaMg<sub>1/3</sub>Ta<sub>2/3</sub>O<sub>3</sub>. *J Eur Ceram Soc*. 2014;34:1741-1753.
44. Moulson AJ, Herbert JM. Electroceramics: materials, properties, applications. John Wiley & Sons. 2003:42-43.

**Table 1.** The calculated fitting parameters  $N_d$ ,  $\tau_0$ , and  $W$  obtained for the three fitted peaks maximized at  $T_{\max}$  with their associated loss tangent at  $T_{\max}$  ( $\tan \delta_{\max}$ ) and the extent of contribution of each dipole relaxation to dielectric constant ( $\Delta\epsilon$ ).

	$T_{\max}$ (K)	$W$ (meV)	$\tau_0$ (s)	$N_d$ (cm <sup>-3</sup> )		$\tan \delta_{\max}$		$\Delta\epsilon$	
				CE0.04	CD0.02	CE0.04	CD0.02	CE0.04	CD0.02
<b>Peak 1</b>	25-30	2.1-6.3	3.4×10 <sup>-11</sup> - 2.1×10 <sup>-10</sup>	23×10 <sup>+16</sup>	6.3×10 <sup>+16</sup>	26×10 <sup>-5</sup>	8.9×10 <sup>-5</sup>	0.022	0.0067
<b>Peak 2</b>	90	32.0-40.1	8.6×10 <sup>-13</sup> - 1.9×10 <sup>-12</sup>	9.0×10 <sup>+16</sup>	6.3×10 <sup>+16</sup>	10×10 <sup>-5</sup>	5.2×10 <sup>-5</sup>	0.0026	0.0018
<b>Peak 3</b>	250	61.0-63.3	6×10 <sup>-12</sup> - 8.6×10 <sup>-12</sup>	90×10 <sup>+16</sup>	27×10 <sup>+16</sup>	21×10 <sup>-5</sup>	8.7×10 <sup>-5</sup>	0.0094	0.0028

## Figure Captions

**Fig. 1.** Temperature dependence of the dielectric loss for (a) CE0.04, (b) ST, and (c) CD0.02 samples at 0 T and 5 T magnetic fields. The insets show loss tangent curves measured at 5 T field in a magnified y-axis to clearly see  $\tan \delta$  features. (d) Difference in loss tangent  $\Delta \tan \delta$  between 0 and 5 T field dielectric loss data for CD0.02 sample. The  $\Delta \tan \delta$  data were fitted by a Curie-Weiss type relation,  $\tan \delta = \frac{a}{T-c} + b$  and two Gaussian peaks (Peak A and Peak B) to obtain the best fit. Resonant frequencies for CE0.04, ST, and CD0.02 samples were 10.5 GHz, 11.6 GHz, and 10.4 GHz, respectively.

**Fig. 2.** Magnetic field dependence of the dielectric loss for CD0.02 sample at 300 K and 20 K.



**Fig. 3.** (a) Temperature dependence of the dielectric loss measured at 5 T magnetic field for CE0.04, ST, and CD0.02 samples. For comparison the measured loss of samples with the intrinsic loss, the estimated intrinsic loss curve is also depicted. (b) Co-excessive and Co-deficient regions around stoichiometric  $\text{Ba}(\text{Co}_{1/3}\text{Nb}_{2/3})\text{O}_3$  composition. Small black dots indicate the target sample compositions on the  $\text{Ba}_3\text{CoNb}_2\text{O}_9$ - $\text{Ba}_5\text{Nb}_4\text{O}_{15}$  and  $\text{Ba}_3\text{CoNb}_2\text{O}_9$ -CoO tie lines in the BaO-CoO-Nb<sub>2</sub>O<sub>5</sub> phase diagram.

**Fig. 4.** Temperature dependence of dielectric loss for (a) CE0.04, (b) ST, and (c) CD0.02 samples. The experimental loss tangent data was fitted by three Debye type dielectric loss peaks; Peak 1 (dashed curve), Peak 2 (dash-dotted curve), and Peak 3 (dotted curve). The solid-purple curve shows the estimated intrinsic loss. Sum of Peak 1, Peak 2, Peak 3, and intrinsic loss curves is depicted with solid-light blue curve for each sample.

**Fig. 5.** (a) Molar susceptibility of CE0.04, ST, and CD0.02 samples as a function of temperature. The inset shows magnified version of a part of susceptibility curves. (b) and (c)  $1/\chi$  curves and the obtained fitted curves on the experimental data for CE0.04 and CD0.02 samples, respectively. (d) the calculated fraction of  $\text{Co}^{2+}$  and  $\text{Co}^{3+}$  cations in 1 mole Co ions.

**Fig. 6.** (a) Arrhenius curve of CE0.04, ST, and CD0.02 samples as a function of temperature. (b) and (c) the magnitude of Peak 1 and Peak 2 versus D.C. conductivity at 873 K and room temperature loss tangent, respectively.

